Enhanced Electrical Conductivity of Imidazolium-Based Ionic Liquids Mixed with Carbon Nanotubes: A Spectroscopic Study

Pablo F. Salazar,[a] Kevin J. Chan,[b] Sai T. Stephens,[a] and Baratunde A. Cola[a,b,*,z]

[a]*George W. Woodruff School of Mechanical Engineering, Georgia Institute of Technology, Atlanta, Georgia 30332, USA*
[b]*School of Materials Science and Engineering, Georgia Institute of Technology, Atlanta, Georgia 30332, USA*

We studied imidazolium-based ionic liquids mixed with multiwall carbon nanotubes using impedance spectroscopy and nuclear magnetic resonance. The results show a percolation threshold below 1 wt% of carbon nanotubes, which, due to their high dispersibility in imidazolium-based ionic liquids, is 3- to 8-fold lower than the percolation threshold for carbon nanotubes in typical organic solvents. The addition of carbon nanotubes appears to polarize their interface with imidazolium-based ionic liquids and increases the diffusion coefficient of the anions up to 35%, which is likely due to weak van der Waals interactions between the carbon nanotube walls and the cations. These effects produce a 3- to 5-fold increase in electrical conductivity of the electrolyte mixture, at carbon nanotube concentrations that are under the threshold for percolation.
 [DOI: 10.1149/2.0401409jes]

Manuscript submitted March 24, 2014; revised manuscript received May 5, 2014. Published June 3, 2014. This was Paper 2609 presented at the San Francisco, California, Meeting of the Society, October 27–November 1, 2013.

Carbon nanotubes (CNTs) in ionic liquids (CNT-ILs) have been proposed recently as electrolytes for dye solar cells (DSCs),[1–4] electrodes for biosensors,[5] electronic materials for flexible actuators,[6] and other applications.[7–9] In particular, mixing single- or multiwall CNTs in iodine-free DSCs can increase energy conversion efficiency by 100 to 300%.[2,4] For example, Lee et al[4] mixed single-wall CNTs (SWCNTs) in 1-ethyl-3-methylimidazolium iodide to reach an efficiency of 1.9%, compared to 0.4% without SWCNTs. The room-temperature stability of their DSCs, with SWCNTs in the IL, is also reported to be superior to that of conventional DSCs, which use I^-/I_2 in an organic solvent. While CNT-ILs show promise to enhance the efficiency of DSCs, the molecular mechanisms that enable the improved performance are not completely clear.[10] Moreover, the solubility of CNTs in ILs, and the compatibility of the mixture, is a processing challenge for several applications.[7,8,11] Because CNT-ILs are mixed ionic-electronic conductors, it is necessary to study the electronic contribution of the ions and CNTs systemically before many applications could be realized. These contributions must be examined above and below the threshold for CNT percolation to fully understand the system, but we found no studies of this type in the literature.

CNTs typically agglomerate in solution and bundle by van der Waals forces.[12] However, some ILs have a high affinity to disperse bundles of CNTs.[9,13–16] Further, ILs are less volatile and toxic[17–19] than conventional solvents used to disperse CNTs without surfactants, such as N-Methyl-2-pyrrolidone (NMP) or dimethylformamide (DMF).[20,21] Despite significant interest in CNT-ILs, the type of molecular interactions between ILs and CNTs are still controversial.[9] While some authors have suggested cation-π interactions between imidazolium-cation ILs and CNTs,[14,22] others have indicated weak van der Waals interactions instead.[23]

Here we use electrochemical impedance spectroscopy (EIS) to quantify the ionic and electronic contributions in the total electrical conductivity of 1-methyl-3-propylimidazolium iodide ([PMIM][I]), 1-butyl-3-methylimidazolium hexafluorophosphate ([BMIM][PF_6]), and 1-butyl-3-methylimidazolium hydrogen sulfate ([BMIM][HSO_4]) mixed with multiwall CNTs (MWCNTs) or nitrogen-doped MWCNTs (N-MWCNTs) below and above the wt% required for percolation. We compare these results to mixtures of MWCNTs in the organic solvents DMF and dimethyl sulfoxide (DMSO). We then use nuclear magnetic resonance (NMR) spectroscopy to reveal the molecular interactions between the MWCNTs and ILs, which provide evidence to support the high dispersibility of CNTs in ILs. EIS and NMR results show that CNT-ILs have enhanced conductivity, which provides an alternative explanation for the recent reports of enhanced energy conversion efficiency in devices that use CNT-IL electrolytes.[1–4]

Experimental

We purchased [BMIM][PF_6], [BMIM][HSO_4], and [PMIM][I] (purity >99%) from IOLITEC; DMF and DMSO from Sigma Aldrich; and MWCNTs and N-MWCNTs from US-nano (US4315 and US4882, respectively). According to product specifications, the MWCNTs had a length of 10–20 μm, outside diameter of 50–80 nm, and density of 2.1 g/cm^3. The N-MWCNTs had an approximate length of 35 μm and outside diameter of 20–50 nm and about 3 wt% nitrogen content. The solvents, ILs, and CNTs were used as received.

We stirred each mixture of MWCNT-IL on a hot plate for 30 minutes, then ultrasonicated the mixture for 30 minutes, followed by another stirring step for 15 minutes, with all steps occurring at a temperature of 65°C. The samples were allowed to cool at room temperature for at least 1 hour, followed by 5 minutes of stirring before taking measurements. To test if the MWCNTs re-agglomerate significantly after time, we made measurements within 5 minutes after the final stirring step, and after 6 hours without additional stirring, and the results only varied by about 5%. Typical sample volumes were approximately 6 mL. To increase the wt% of MWCNTs in the ILs, we added MWCNTs to the mixture subsequent to the previous test at lower wt% and repeated the stirring and sonication steps described above. Coulometric Karl Fischer titration (Titroline KF, Schott instruments) indicates water content less than 0.05 wt%, before and after the mixing in the ILs (Table S1). Previous studies on the effect of water impurity showed a change of less than 4% in the electrical conductivity of imidazolium-based ionic liquids when the water content is below 0.1 wt%.[24,25] The electrochemical setup consisted of a 2-electrode configuration with platinum electrodes. The conversion of the measured resistance to conductivity was calibrated using standard solutions of potassium chloride at 0.01 M and 0.1 M, following equations S1 and S2 in the supplemental information. EIS was performed with a CH instruments Model 660E potensiostat. The ac voltage amplitude was 20 mV and the dc signal was 0 mV. The spectra ranged from 1 MHz to 0.02 Hz for all the solvents and ILs, except for [PMIM][I]. We extended the lowest frequency in [PMIM][I] to 0.002 Hz, in order to reach the region where diffusion is dominant. We fit the data to impedance circuit models using the automated software provided by CH instruments.

*Electrochemical Society Active Member.
[z]E-mail: cola@gatech.edu

We performed ^{1}H-1D and ^{1}H-PSGE diffusion NMR spectroscopy of neat MWCNT-ILs in NMR tubes 5 mm in diameter at 23°C, and in a Bruker AV3–400 NMR spectrometer (magnetic field strength of 9.4 T). The instrument was equipped with a Bruker Diff50 diffusion probe and gradient amplifiers allowing pulsed field gradient (PFG) experiments with magnetic field gradients larger than 2000 G/cm. The chemical shift scale was calibrated using an external standard of 0.1% DSS (3-Trimethylsilylpropane sulfonic acid and chemical shift calibrated to 0 ppm) in D_2O containing 20% H_2O. The diffusion coefficients were measured using the PFG stimulated echo sequence (PFG-STE). Spectra were measured as a function of the gradient strength. Integrals over individual peaks were fitted using the Bruker Topsin software according to the Stejskal-Tanner equation:[26–28]

$$\ln\left(\frac{I}{I_o}\right) = -(\gamma\delta)^2 G^2 \left(\Delta - \frac{\delta}{3}\right) D, \qquad [1]$$

where I/I_o is the ratio of the intensities with and without the gradient pulses, γ is the gyromagnetic ratio, G is the gradient strength, Δ is the diffusion time, i.e. the delay between the midpoints of the gradients (50 ms), δ is the gradient duration (2 ms), and D is the diffusion coefficient. The gradient pulses, providing G up to 2000 G/cm, were used for each measurement. Experimental uncertainty is approximately ±4% for the NMR measurements and ±9% for the EIS measurements, based on repeating each experiment three times.

Results and Discussion

Electrochemical impedance spectroscopy.— The impedance spectra for pure solvents or ILs, with the exception of [PMIM][I], resemble that of a dielectric material (Figure 1). As MWCNTs are added, the conductivity of the MWCNT-IL mixtures increases, and the spectra in Figure 1 shift upward. When enough MWCNTs are added to the ILs or solvents to produce a percolated state, the conductivity at low frequencies increases by several orders of magnitude, and the spectrum resembles that of a resistor (frequency independent).

We fit the spectra in Figure 1 to the Debye model[29,30] (Figure 2a) when the MWCNT-IL mixtures are below their percolation threshold – except for the [PMIM][I] spectra, which requires a different model. In the Debye model, a dielectric material is represented by two sets of parallel resistors and capacitors that are connected in series (Figure 2a). The dielectric capacitance between the metal electrodes (C_b) is proportional to the permittivity of the solvent or electrolyte. When an electric field is applied, the ions migrate toward the electrodes, and ion pairs polarize and orient in the direction of the applied field. The mobility of the ions and dipoles, and concentration of charges determine the bulk resistance, R_b. The accumulation of

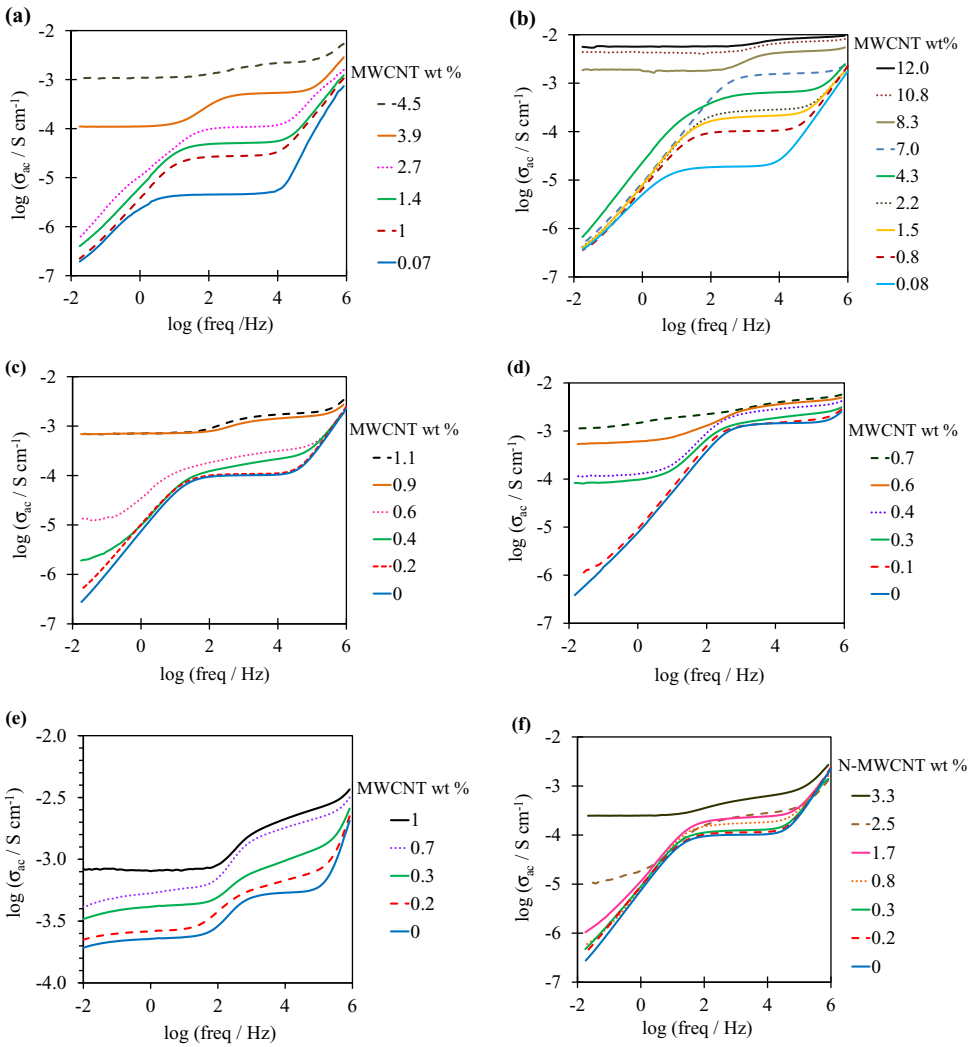

Figure 1. Frequency dependence of ac conductivity, σ_{ac}, for MWCNT powders mixed in DMF (a), DMSO (b), [BMIM][HSO_4] (c), [BMIM][PF_6] (d), [PMIM][I] (e) and [BMIM][HSO_4] mixed with N-MWCNTs (f). The measured impedance spectra are converted to conductivity using equations S1 and S2 in the supplemental information.

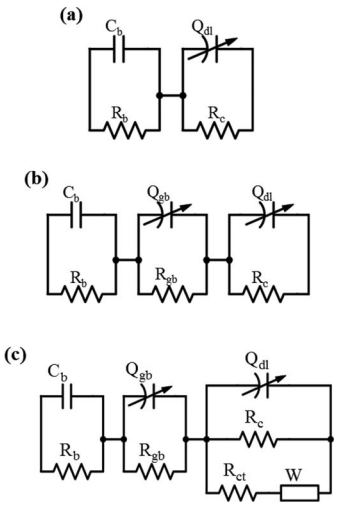

Figure 2. Models used to fit the EIS of MWCNT-ILs. a) Model for a dielectric material. b) Model for a dielectric material with suspended particles forming grain boundaries. c) Model for a redox electrolyte with suspended particles. C_b is the bulk capacitance; R_b is the bulk resistance; Q_{dl} is the double layer capacitance; R_c is the contact resistance; Q_{gb} is the grain boundary capacitance; R_{gb} is the grain boundary resistance; R_{ct} is the charge transfer resistance; and W is the Warburg impedance.

charges at the electrode interface with the electrolyte or solvent is represented by the constant-phase element, Q_{dl}, which is a non-ideal capacitor with a phase between 0 and 90° that accounts for the surface roughness of the electrode and other inhomogeneous properties at the double layer.[31,32] The contact resistance at this interface is R_c.

The two parallel RC brackets connected in series in the model of Figure 2a have different time constants. C_b in parallel with R_b determines the impedance (Z_{HF}) in the high frequency region (>10^4 Hz) as

$$Z_{HF} = \frac{R_b}{1 + j\omega C_b R_b}, \quad [2]$$

where ω is the frequency. Whereas, R_c in parallel with Q_{dl} determines the impedance (Z_{LF}) in the low frequency region (<100 Hz) as

$$Z_{LF} = \frac{R_c}{1 + (j\omega)^{\alpha} Q_{dl} R_c}, \quad [3]$$

where α is the constant-phase element coefficient (between 0 and 1) due to the inhomogeneity of the electrode. The bulk resistance (R_b) determines the frequency independent conductivity in the mid-frequency region of the spectra (between 10^2 and 10^4 Hz).

When the MWCNT-IL mixtures are near and above their percolation threshold, we fit the spectra to the model in Figure 2b to account for the grain boundaries between the MWCNTs and IL.[33,34] The resistance and capacitance at these grain boundaries are represented by R_{gb} and Q_{gb}, respectively. We fit the spectra for the redox IL [PMIM][I] to the model in Figure 2c.[29] The charge transfer resistance, R_{ct}, is due to the activation polarizations of the electrochemical reactions of iodide. The Warburg impedance, W, is the mass transfer impedance due to diffusion near the electrode.

We extract the changes in bulk and contact resistance as MWCNTs are added (Figure 3) by fitting the measured spectra to the models in Figure 2. The fitted parameters are presented in Tables S2 to S7

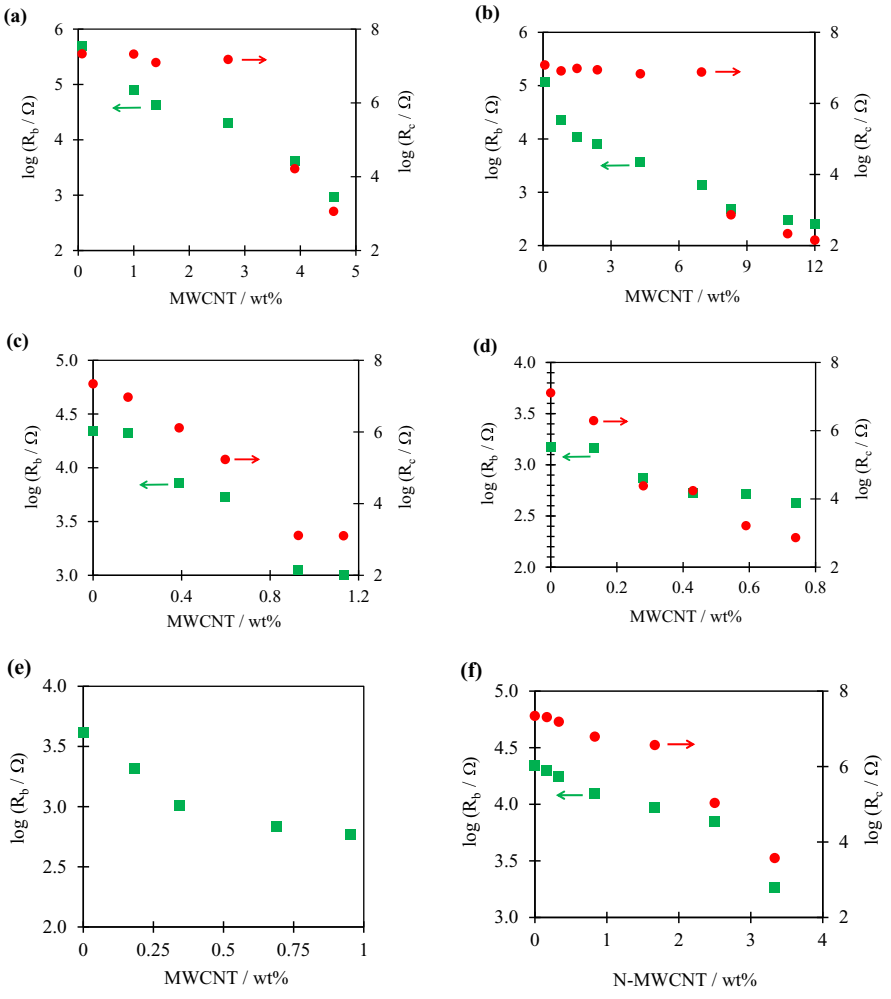

Figure 3. Bulk, R_b (green squares), and contact, R_c (red circles), resistances, as MWCNTs are added in DMF (a), DMSO (b), [BMIM][HSO_4] (c), [BMIM][PF_6] (d), [PMIM][I] (e), and as N-MWCNTs are added to [BMIM][HSO_4] (f). The impedance spectra of Figure 1 are fit with the models in Figure 2 to obtain the resistances.

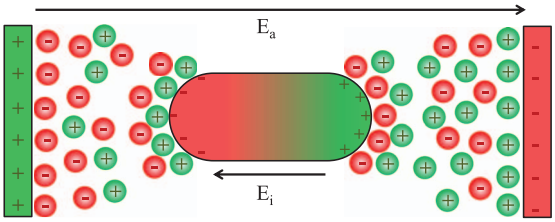

Figure 4. Schematic representation of the interfacial polarization induced in a conductive particle (e.g., MWCNT) in an ionic medium. In addition to ionic diffusion of the positive (+) and negative (-) charges, the applied electric field (E_a) induces an internal electric field (E_i) from the electronic polarization in the particle and redistribution of the ions around the surface.

in the supplemental information. Figure 1 shows that the percolated state in DMF and DMSO is reached around 3 wt% and 8 wt% of MWCNTs, respectively. These percolation thresholds correlate with their low dispersion limits of 2.3×10^{-3} wt% and 5.4×10^{-4} wt%, respectively.[35] A low dispersion limit means that MWCNTs aggregate at low wt%, which decreases the aspect ratio of the particles and results in a high percolation threshold.[36] In the MWCNT-ILs mixtures (Figure 1c, 1d and 1e), the percolation state is reached below 1 wt%. Based on the aspect ratio of the MWCNTs we used, the theoretical critical volume fraction at the percolation threshold for randomly oriented cylinders is between 0.002 and 0.006.[36] The critical volume fraction found from our measurements of MWCNTs in ILs falls between 0.006 and 0.009, suggesting a high affinity of the ILs to disperse the MWCNTs.

Figure 3 shows that before reaching the percolated state, the bulk resistance (R_b) of the MWCNT-IL mixtures drops by 3 to 5 fold. The contact resistance (R_c) drops approximately 3 orders of magnitude, but still remains 1 to 2 orders of magnitude higher than R_b. At the percolated state, R_b and R_c are in the same order of magnitude, approximately 10^3 Ω. Without MWCNTs, R_b and R_c of the ILs depend mainly on their ionic diffusion at the bulk and diffusive boundary layer, respectively. But when MWCNTs are added, interfacial polarization and percolation decrease R_b and R_c.[30,36–38] As shown in Figure 4, when an electric field is applied to a conductive particle (e.g., MWCNTs) in a medium, the particle is polarized. Then, the charges in the medium redistribute around the particle in accordance with Coulomb's law (i.e., Maxwell-Wagner polarization or interfacial polarization). As the dipoles near the particle orient in the direction of the electric field, they absorb energy that otherwise would be stored in the dielectric. Adding MWCNTs to the solutions increases the interfacial area over which the dipoles orient and, thus, reduces the ohmic resistance by increasing the dielectric loss.[34,37,39]

Nuclear magnetic resonance.— We chose [BMIM][HSO_4] for NMR studies because the imidazolium cation and anion contain the same NMR-sensitive isotope (^{1}H) (Figure 5a), which allows us to study the effects of adding MWCNTs on both the cation and anion. In the neat [BMIM][HSO_4] spectrum (bottom curve of Figure 5b) the peak around 10.4 ppm belongs to the anion isotope, while the others correspond to the cation. The peak assignments were validated according to other NMR studies in neat ILs.[40–42] As MWCNTs are added to [BMIM][HSO_4] (top 3 spectra on Figure 5b) there is a broadening of all the peaks. The broadening is likely due to inhomogeneous local magnetic fields caused by the nanoparticles.[43] A close look at the peak positions (Figure 5c-5e) shows a slight deshielding (shift to higher ppm) of all the cation peaks proportional with the concentration of MWCNTs. The shifts of peaks 5–6 (close ups of these are not shown) are similar to the shifts of peaks 7–9. The anion peak, however, remains almost at the same shift.

The [BMIM][HSO_4] cation-peak shifts suggest weak van der Waals interactions between the cations and the MWCNTs.[16,23] The possibility of cation-π interaction or electrostatic interactions, as suggested by some authors,[14,22] would mean a stronger shift of the hydrogen isotopes in the imidazolium ring, as they concentrate most of the positive charge. Thus, according to the spectra in Figure 5c-5e, the cation-π interaction or electrostatic interactions between the MWCNTs and cations do not appear to occur.

The diffusion coefficients of the hydrogen isotopes are shown in Figure 6. The diffusion coefficient of the anions increases as

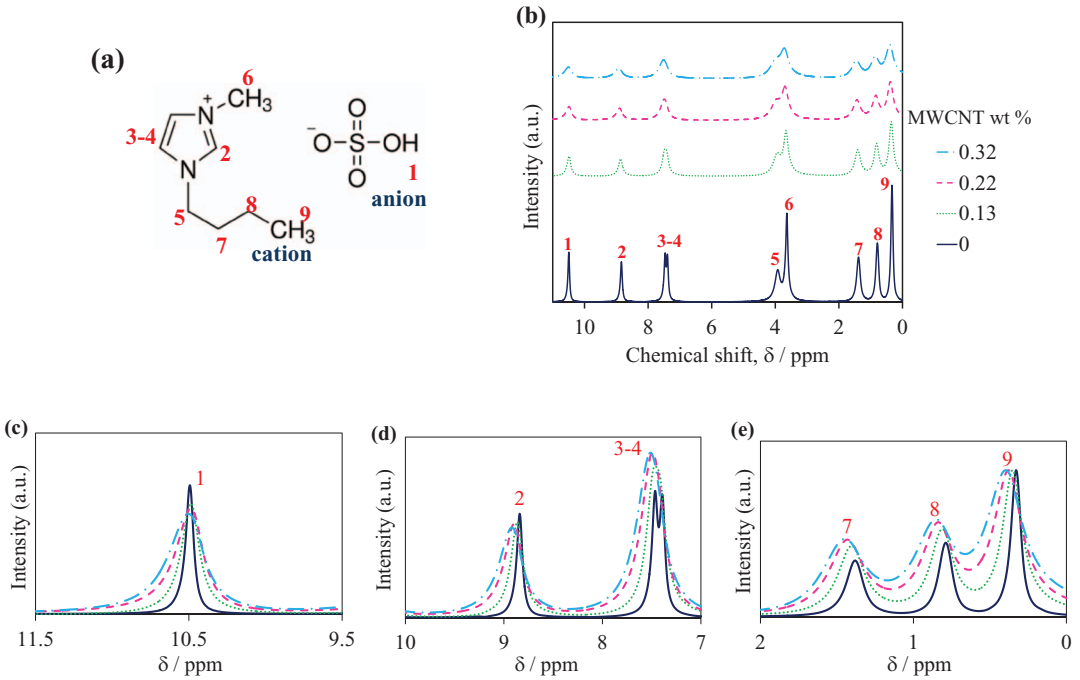

Figure 5. a) Molecular structure of [BMIM][HSO_4] and hydrogen assignments. b) ^{1}H NMR spectroscopy of neat [BMIM][HSO_4] (dark blue), and MWCNT-[BMIM][HSO_4] mixtures with MWCNTs at 0.13 wt% (green), 0.22 wt% (purple) and 0.32 wt% (light blue). Close up plots of the ^{1}H spectra are shown in c, d, and e. The intensities are normalized with respect to the peak height at ~0.3 ppm (i.e., peak 9).

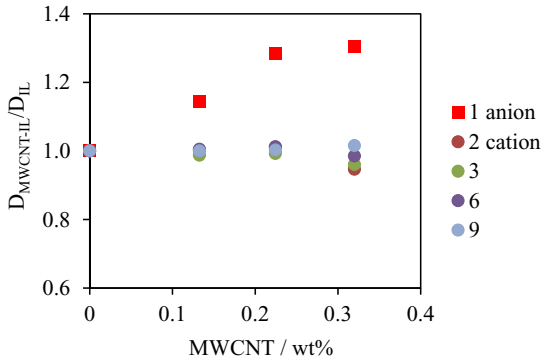

Figure 6. Diffusion coefficients of [BMIM][HSO_4] mixed with MWCNTs from pulse gradient spin-echo NMR spectroscopy. $D_{MWCNT-IL}/D_{IL}$ is the ratio of the diffusion coefficient in the MWCNT-IL mixture and in the neat IL. Labels 1 through 9 correspond to the diffusion coefficients of the ^{1}H isotopes of the anion and cation shown in Figure 5a.

MWCNTs are added. However, the diffusion coefficients of the larger cations, decrease, probably because the IL becomes more viscous with the addition of MWCNTs.[44–47] These trends provide additional evidence that weak van der Waals interactions occur between the cations of the IL and MWCNTs. A possible explanation for the increase in the diffusion coefficient of the anions is that, when the cations become attracted to the walls of the MWCNTs, some of the ion pairs are broken, which releases the anions and increases their diffusion coefficient.

To further study the type of interaction between the imidazolium-ILs and the MWCNTs, we test the effect of increased negative charge in the MWCNTs on their ability to break ion pairs. We performed similar NMR studies with N-MWCNTs in [BMIM][HSO_4]. The diffusion coefficient of the anions also increases with the concentration of N-MWCNTs (Figure 7a), but to a lesser degree than with pristine MWCNTs. In addition, Figures 7c-7e show a smaller shift of the cation peaks, compared to pristine MWCNTs, as N-MWCNTs are added to [BMIM][HSO_4]. This result suggests weaker van der Waals interaction between the N-MWCNT and the IL cations compared to the cation interaction with pristine MWCNTs, which results in less breaking of ion pairs. This weaker attraction is likely due to the smaller van der Waal radii of nitrogen compared to carbon.[48] For both MWCNTs and N-MWCNTs, there is not a significant shift of the peaks of the imidazolium ring exclusively, as would be expected in cation-π interactions, which adds further evidence to support our hypothesis of van der Waals interactions between the MWCNT walls and the IL.

Conclusions

We report lower percolation thresholds of MWCNTs in [BMIM][PF_6], [BMIM][HSO_4] and [PMIM][I], than in organic solvents (DMF and DMSO), using electrochemical impedance spectroscopy. These results provide clear evidence for the high dispersibility of MWCNTs in imidazolium-based ILs. This high dispersibility is likely the result of weak van der Waals interactions between the MWCNT walls and imidazolium cations, as indicated by nuclear magnetic resonance spectroscopy. Using diffusion nuclear magnetic resonance, we show that only the diffusion coefficient of the anions increases as MWCNTs are added to the ILs. In addition, adding MWCNTs to the ILs increases interfacial polarization in the MWCNT-IL mixtures, which, when combined with the increased diffusion coefficient of the anion, decreased the bulk resistance of the mixtures by 3 to 5-fold, before reaching the percolated state. This work suggests that engineering MWCNT-IL mixtures to maximize interfacial polarization, while avoiding a fully percolated state, which could reduce the cell voltage, could produce a new class of low-resistance electrolytes for increased efficiency in a host of applications that use electrochemical energy conversion.

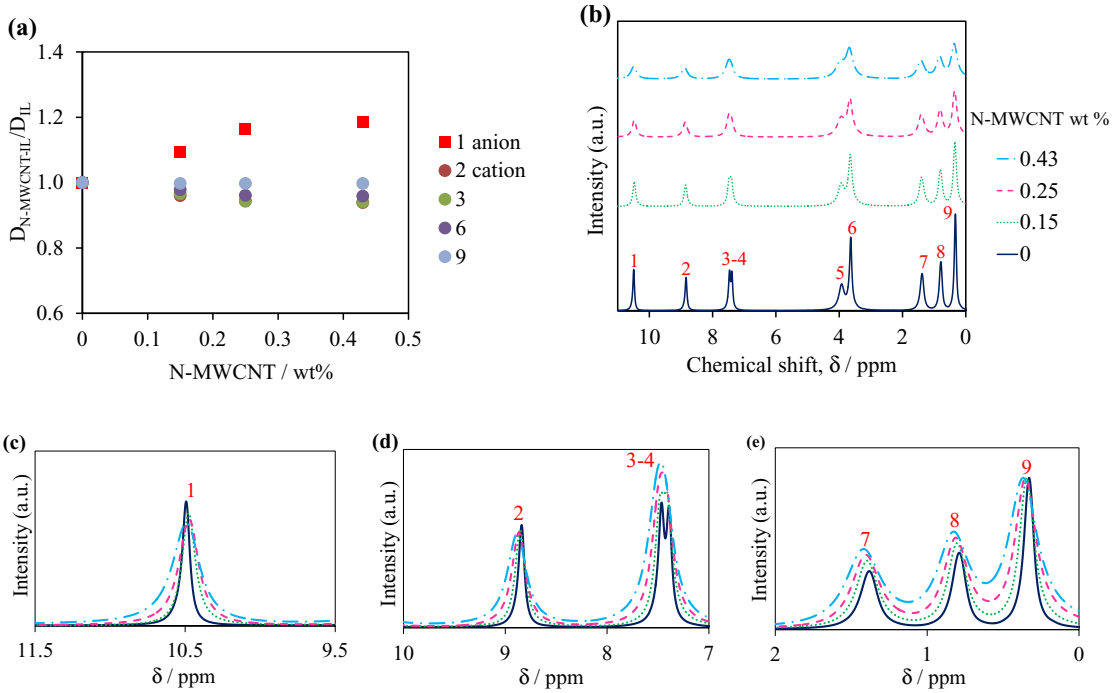

Figure 7. a) Diffusion coefficients of [BMIM][HSO_4] mixed with N-MWCNTs from pulse gradient spin-echo NMR spectroscopy. $D_{N-MWCNT-IL}/D_{IL}$ is the ratio of the diffusion coefficient in the N-MWCNT-IL mixture and in the neat IL. Labels 1 through 9 correspond to the diffusion coefficients of the ^{1}H isotopes of the anion and cation shown in Figure 5a. b) ^{1}H NMR spectroscopy of neat [BMIM][HSO_4] (dark blue), and N-MWCNT-[BMIM][HSO_4] mixtures with N-MWCNTs at 0.15 wt% (green), 0.25 wt% (purple) and 0.43 wt% (light blue). Close up plots of the ^{1}H spectra are shown in c, d, and e. The intensities are normalized with respect to the peak height at ~0.3 ppm (i.e., peak 9).

Acknowledgments

We are grateful for the financial support of National Science Foundation Award No. CBET 1055479. We also thank Dr. Johannes Leisen for his help with collecting nuclear magnetic resonance data. K. J. Chan's work was supported by a summer undergraduate research fellowship (SURF).

References

1. J. E. Benedetti, A. A. Corrêa, M. Carmello, L. C. P. Almeida, A. S. Gonçalves, and A. F. Nogueira, *Journal of Power Sources*, **208**(0), 263 (2012).
2. Y.-H. Chang, P.-Y. Lin, S.-R. Huang, K.-Y. Liu, and K.-F. Lin, *Journal of Materials Chemistry*, **22**(31), 15592 (2012).
3. M. R. Karim, A. Islam, S. P. Singh, and L. Han, *Advances in OptoElectronics*, **2011**, 7 (2011).
4. C.-P. Lee, L.-Y. Lin, P.-Y. Chen, R. Vittal, and K.-C. Ho, *Journal of Materials Chemistry*, **20**(18), 3619 (2010).
5. Y. Zhang, Y. Shen, D. Han, Z. Wang, J. Song, F. Li, and L. Niu, *Biosensors and Bioelectronics*, **23**(3), 438 (2007).
6. T. Fukushima, K. Asaka, A. Kosaka, and T. Aida, *Angewandte Chemie*, **117**(16), 2462 (2005).
7. T. Fukushima and T. Aida, *Chemistry – A European Journal*, **13**(18), 5048 (2007).
8. M. Tunckol, J. Durand, and P. Serp, *Carbon*, **50**(12), 4303 (2012).
9. Y.-K. Yang, X.-L. Xie, and W. Cui, in *Green Solvents II*, A. Mohammad and D. Inamuddin, eds., p. 399-434, Springer Netherlands, (2012).
10. H. Vahlman, J. Halme, J. Korhonen, K. Aitola, and J. Patakangas, *The Journal of Physical Chemistry C*, **117**(23), 11920 (2013).
11. D. F. Aaron, *Nature*, **498**(7455), 443 (2013).
12. A. Thess, R. Lee, P. Nikolaev, and H. Dai, *Science*, **273**(5274), 483 (1996).
13. M. L. Polo-Luque, B. M. Simonet, and M. Valcárcel, *TrAC Trends in Analytical Chemistry*, **47**(0), 99 (2013).
14. T. Fukushima, A. Kosaka, Y. Ishimura, T. Yamamoto, T. Takigawa, N. Ishii, and T. Aida, *Science*, **300**(5628), 2072 (2003).
15. J. B. Ducros, N. Buchtova, A. Magrez, O. Chauvet, and J. Le Bideau, *Journal of Materials Chemistry*, **21**(8), 2508 (2011).
16. C. J. Jameson, *Bulletin of Magnetic Resonance*, **3**(1), 3 (1980).
17. C. P. Fredlake, J. M. Crosthwaite, D. G. Hert, S. N. V. K. Aki, and J. F. Brennecke, *Journal of Chemical & Engineering Data*, **49**(4), 954 (2004).
18. M. Galiński, A. Lewandowski, and I. Stępniak, *Electrochimica Acta*, **51**(26), 5567 (2006).
19. R. Martínez-Palou, *Mol Divers*, **14**(1), 3 (2010).
20. K. D. Ausman, R. Piner, O. Lourie, R. S. Ruoff, and M. Korobov, *The Journal of Physical Chemistry B*, **104**(38), 8911 (2000).
21. G. Chen, G. Sun, and Z. Liu, *Nano*, **05**(02), 103 (2010).
22. S. Bellayer, J. W. Gilman, N. Eidelman, S. Bourbigot, X. Flambard, D. M. Fox, H. C. De Long, and P. C. Trulove, *Advanced Functional Materials*, **15**(6), 910 (2005).
23. J. Wang, H. Chu, and Y. Li, *ACS Nano*, **2**(12), 2540 (2008).
24. J. A. Widegren and J. W. Magee, *Journal of Chemical and Engineering Data*, **52**(6), 2331 (2007).
25. J. A. Widegren, E. M. Saurer, K. N. Marsh, and J. W. Magee, *The Journal of Chemical Thermodynamics*, **37**(6), 569 (2005).
26. W. S. Price, *Concepts in Magnetic Resonance*, **9**(5), 299 (1997).
27. W. S. Price, *Concepts in Magnetic Resonance*, **10**(4), 197 (1998).
28. M. A. B. H. Susan, A. Noda, and M. Watanabe, in *Electrochemical Aspects of Ionic Liquids*, p. 55-74, John Wiley & Sons, Inc., (2005).
29. V. F. Lvovich, in *Impedance Spectroscopy - Applications to Electrochemical and Dielectric Phenomena*, p. 97-111, John Wiley & Sons, (2012).
30. J. Zhang, M. Mine, D. Zhu, and M. Matsuo, *Carbon*, **47**(5), 1311 (2009).
31. J.-B. Jorcin, M. E. Orazem, N. Pébère, and B. Tribollet, *Electrochimica Acta*, **51**(8–9), 1473 (2006).
32. V. F. Lvovich, *Impedance Spectroscopy - Applications to Electrochemical and Dielectric Phenomena*, John Wiley & Sons (2012).
33. J. Jankovic, D. P. Wilkinson, and R. Hui, *Journal of The Electrochemical Society*, **159**(2), B109 (2011).
34. V. F. Lvovich, in *Impedance Spectroscopy - Applications to Electrochemical and Dielectric Phenomena*, p. 113-144, John Wiley & Sons, (2012).
35. Q. Cheng, S. Debnath, L. O'Neill, T. G. Hedderman, E. Gregan, and H. J. Byrne, *The Journal of Physical Chemistry C*, **114**(11), 4857 (2010).
36. W. Bauhofer and J. Z. Kovacs, *Composites Science and Technology*, **69**(10), 1486 (2009).
37. G. M. Tsangaris, N. Kouloumbi, and S. Kyvelidis, *Materials Chemistry and Physics*, **44**(3), 245 (1996).
38. Y. Xi, Y. Bin, C. K. Chiang, and M. Matsuo, *Carbon*, **45**(6), 1302 (2007).
39. C. P. Smyth, *Dielectric behavior and structure: dielectric constant and loss, dipole moment and molecular structure*, McGraw-Hill (1955).
40. F. Cesare Marincola, C. Piras, O. Russina, L. Gontrani, G. Saba, and A. Lai, *ChemPhysChem*, **13**(5), 1339 (2012).
41. Y. Jeon, J. Sung, C. Seo, H. Lim, H. Cheong, M. Kang, B. Moon, Y. Ouchi, and D. Kim, *The Journal of Physical Chemistry B*, **112**(15), 4735 (2008).
42. Y.-Z. Zheng, N.-N. Wang, J.-J. Luo, Y. Zhou, and Z.-W. Yu, *Physical Chemistry Chemical Physics*, **15**(41), 18055 (2013).
43. T. D. W. Claridge, *High-resolution NMR techniques in organic chemistry*, Elsevier, Amsterdam (2009).
44. H. Chen, Y. Ding, Y. He, and C. Tan, *Chemical Physics Letters*, **444**(4–6), 333 (2007).
45. J.-H. Lee, K. S. Hwang, S. P. Jang, B. H. Lee, J. H. Kim, S. U. S. Choi, and C. J. Choi, *International Journal of Heat and Mass Transfer*, **51**(11–12), 2651 (2008).
46. P.-C. Ma, *Carbon Nanotubes for Polymer Reinforcement*, CRC Press, London, GBR (2011).
47. H. Usui, H. Matsui, N. Tanabe, and S. Yanagida, *Journal of Photochemistry and Photobiology A: Chemistry*, **164**(1–3), 97 (2004).
48. W. M. Haynes, *CRC Handbook of Chemistry and Physics*, 93rd Edition, Taylor & Francis (2012).

Supplemental Information for:

Enhanced Electrical Conductivity of Imidazolium-based Ionic Liquids Mixed with Carbon Nanotubes: A Spectroscopic Study

Pablo F. Salazar[1], Kevin J. Chan[2], Sai T. Stephens[1] and Baratunde A. Cola[1,2,a]

[1]George W. Woodruff School of Mechanical Engineering, Georgia Institute of Technology, Atlanta, Georgia 30332.

[2]School of Materials Science and Engineering, Georgia Institute of Technology, Atlanta, Georgia 30332.

[a]Corresponding author: cola@gatech.edu

Water content measurements

Table S1. Water content (wt%) in [BMIM][PF_6], [BMIM][HSO_4] and [PMIM][I], before and after the mixing procedure.

	Before	After
[BMIM][PF_6]	0.033	0.011
[BMIM][HSO_4]	0.021	0.017
[PMIM][I]	0.01	0.017

Calibration of the conductivity measurements

Because of edge effects, the electric flux will not be entirely uniform between the electrodes. The conversion from the measured resistance to conductivity is obtained by using a standard electrolyte solutions aqueous KCl solution at 0.1 M or 0.01 M [11]. We define the geometry factor of cell (*GF*) as

$$GF = \frac{1}{\sigma_{\mathrm{KCl}} R_{\mathrm{KCl}}}, \tag{S1}$$

where σ_{KCl} is the conductivity reported for KCl and R_{KCl} is the measured resistance. Then, the resistivity of the new electrolyte is

$$\frac{1}{\sigma_{\text{electrolyte}}} = (GF)R_{\text{electrolyte}} . \quad \text{(S2)}$$

Fitting parameters of the impedance spectra

Table S2. Fitting parameters of the impedance spectra in MWCNT-DMF mixtures to the model in Figure 2a. C_b is the bulk capacitance; R_b is the bulk resistance; Q_{dl} is the double layer capacitance; α_{dl} is the constant phase element coefficient for Q_{dl}; and R_c is the contact resistance.

MWCNT wt%	R_b (Ω)	R_c (Ω)	C_b (Ω^{-1}s)	Q_{dl} ($\Omega^{-1}s^{\alpha dl}$)	α_{dl}
0.07	4.9×10^5	2.1×10^7	5.3×10^{-10}	3.6×10^{-7}	0.81
1	7.9×10^4	2.1×10^7	1.2×10^{-10}	4.2×10^{-7}	0.82
1.4	4.3×10^4	1.2×10^7	1.7×10^{-10}	5.4×10^{-7}	0.85
2.7	2.0×10^4	1.5×10^7	2.9×10^{-10}	1.5×10^{-6}	0.83
3.9	4.1×10^3	1.6×10^4	3.0×10^{-10}	9.5×10^{-7}	0.83
4.5	9.3×10^2	1.1×10^3	8.7×10^{-10}	1.2×10^{-5}	0.60

Table S3. Fitting parameters of the impedance spectra in MWCNT-DMSO mixtures to the model in Figure 2b. C_b is the bulk capacitance; R_b is the bulk resistance; Q_{dl} is the double layer capacitance; α_{dl} is the constant phase element coefficient for Q_{dl}; and R_c is the contact resistance.

MWCNT wt%	R_b (Ω)	R_c (Ω)	C_b ($\Omega^{-1}s$)	Q_{dl} ($\Omega^{-1}s^{\alpha dl}$)	α_{dl}
0.08	1.2×10^5	1.2×10^7	1.3×10^{-10}	6.2×10^{-7}	0.77
0.8	2.2×10^4	8.2×10^6	1.9×10^{-10}	6.0×10^{-7}	0.88
1.5	1.1×10^4	9.6×10^6	2.1×10^{-10}	7.7×10^{-7}	0.86
2.4	8.0×10^3	8.8×10^6	2.1×10^{-10}	7.6×10^{-7}	0.85
4.3	3.6×10^3	6.8×10^6	2.7×10^{-10}	2.1×10^{-6}	0.85
7.0	1.4×10^3	7.6×10^6	2.2×10^{-10}	8.9×10^{-7}	0.86
8.3	4.9×10^2	7.3×10^2	7.4×10^{-10}	9.1×10^{-7}	0.88
10.8	3.1×10^2	2.2×10^2	1.4×10^{-9}	2.6×10^{-6}	0.80
12.0	2.5×10^2	1.4×10^2	1.1×10^{-9}	4.6×10^{-6}	0.80

Table S4. Fitting parameters of the impedance spectra in MWCNT-[BMIM][HSO_4] mixtures to the model in Figure 2c, except at low concentrations of MWCNTs, at which grain boundaries effects were small. C_b is the bulk capacitance; R_b is the bulk resistance; Q_{dl} is the double layer capacitance; α_{dl} is the constant phase element coefficient for Q_{dl}; R_c is the contact resistance; Q_{gb} is the grain boundary capacitance; α_{gb} is constant phase element coefficient for Q_{gb}; and R_{gb} is the grain boundary resistance.

MWCNT wt%	R_b (Ω)	R_c (Ω)	C_b ($\Omega^{-1}s$)	Q_{dl} ($\Omega^{-1}s^{\alpha dl}$)	α_{dl}	R_{gb} (Ω)	Q_{gb} ($\Omega^{-1}s^{\alpha gb}$)	α_{gb}
0	2.2×10^4	2.2×10^7	2.0×10^{-10}	6.9×10^{-7}	0.86			
0.2	2.1×10^4	9.3×10^6	1.9×10^{-10}	1.0×10^{-6}	0.83			
0.4	7.2×10^3	1.3×10^6	2.9×10^{10}	1.1×10^{-6}	0.80	1.1×10^4	3.8×10^{-6}	0.37
0.6	5.3×10^3	1.7×10^5	2.2×10^{-10}	3.7×10^{-6}	0.86	1.5×10^4	8.2×10^{-6}	0.36
0.9	1.1×10^3	1.3×10^3	2.7×10^{-10}	1.6×10^{-6}	0.84	7.4×10^2	1.8×10^{-5}	0.37
1.1	1.0×10^3	1.3×10^3	2.7×10^{-10}	1.8×10^{-6}	0.84	8.0×10^2	6.4×10^{-5}	0.37

Table S5. Fitting parameters of the impedance spectra in MWCNT-[BMIM][PF_6] mixtures to the model in Figure 2d, except at low concentrations of MWCNTs, at which grain boundaries effects were small. C_b is the bulk capacitance; R_b is the bulk resistance; Q_{dl} is the double layer capacitance; α_{dl} is the constant phase element coefficient for Q_{dl}; R_c is the contact resistance; Q_{gb} is the grain boundary capacitance; α_{gb} is constant phase element coefficient for Q_{gb}; and R_{gb} is the grain boundary resistance.

MWCNT wt%	R_b (Ω)	R_c (Ω)	C_b ($\Omega^{-1}s$)	Q_{dl} ($\Omega^{-1}s^{\alpha dl}$)	α_{dl}	R_{gb} (Ω)	Q_{gb} ($\Omega^{-1}s^{\alpha gb}$)	α_{gb}
0	1.5×10^3	1.3×10^7	2.1×10^{-10}	8.5×10^{-7}	0.83			
0.1	1.4×10^3	2.0×10^6	3.6×10^{-10}	8.5×10^{-7}	0.86			
0.3	7.4×10^2	2.4×10^4	3.4×10^{-10}	1.8×10^{-6}	0.86	7.9×10^2	2.0×10^{-5}	0.37
0.4	5.3×10^2	1.7×10^4	2.8×10^{-10}	1.6×10^{-6}	0.86	5.2×10^2	2.7×10^{-5}	0.37
0.6	5.2×10^2	1.6×10^3	7.3×10^{-10}	5.6×10^{-6}	0.80	2.2×10^3	1.3×10^{-4}	0.37
0.7	4.2×10^2	7.3×10^2	6.2×10^{-10}	4.2×10^{-4}	0.80	9.5×10^2	2.6×10^{-5}	0.45

Table S6. Fitting parameters of the impedance spectra in MWCNT-[PMIM][I] mixtures to the model in Figure 2e. R_c was not found below percolation because the model was overdetermined. C_b is the bulk capacitance; R_b is the bulk resistance; Q_{dl} is the double layer capacitance; α_{dl} is the constant phase element coefficient for Q_{dl}; R_c is the contact resistance; Q_{gb} is the grain boundary capacitance; α_{gb} is the constant phase element coefficient for Q_{gb}; R_{gb} is the grain boundary resistance; R_{ct} is the charge transfer resistance; and W is the Warburg impedance.

MWCNT wt%	R_b (Ω)	R_{CT} (Ω)	C_b ($\Omega^{-1}s$)	Q_{dl} ($\Omega^{-1}s^{\alpha dl}$)	α_{dl}	R_{gb} (Ω)	Q_{gb} ($\Omega^{-1}s^{\alpha gb}$)	α_{gb}	W ($\Omega s^{-0.5}$)	R_c (Ω)
0	4.1×10^3	5.5×10^3	2.1×10^{-10}	5.4×10^{-7}	0.87				1.4×10^{-3}	
0.2	2.1×10^3	3.9×10^3	2.8×10^{-10}	1.2×10^{-6}	0.87	2.4×10^3	7.0×10^{-6}	0.37	1.7×10^{-3}	
0.3	1.0×10^3	2.2×10^3	3.6×10^{-10}	1.1×10^{-6}	0.89	2.1×10^3	5.9×10^{-6}	0.37	1.9×10^{-3}	
0.7	6.8×10^2	2.4×10^3	3.4×10^{-10}	1.2×10^{-6}	0.87	9.0×10^2	1.3×10^{-5}	0.36	2.2×10^{-3}	
1.0	5.9×10^2		4.6×10^{-10}	9.5×10^{-7}	0.89	1.1×10^3	2.0×10^{-5}	0.37	IND	1.6×10^3

Table S7. Fitting parameters of the impedance spectra in N-MWCNT-[BMIM][HSO_4] mixtures to the model in Figure 2f, except at low concentrations of N-MWCNTs, at which grain boundaries effects were small. C_b is the bulk capacitance; R_b is the bulk resistance; Q_{dl} is the double layer capacitance; α_{dl} is the constant phase element coefficient for Q_{dl}; R_c is the contact resistance; Q_{gb} is the grain boundary capacitance; α_{gb} is constant phase element coefficient for Q_{gb}; and R_{gb} is the grain boundary resistance.

N-MWCNT wt%	R_b (Ω)	R_c (Ω)	C_b ($\Omega^{-1}s$)	Q_{dl} ($\Omega^{-1}s^{\alpha dl}$)	α_{dl}	R_{gb} (Ω)	Q_{gb} ($\Omega^{-1}s^{\alpha gb}$)	α_{gb}
0	2.2×10^4	2.2×10^7	2.0×10^{-10}	6.9×10^{-7}	0.86			
0.2	2.0×10^4	2.0×10^7	1.9×10^{-10}	9.4×10^{-7}	0.82			
0.3	1.7×10^4	1.5×10^7	1.9×10^{-10}	1.0×10^{-6}	0.82			
0.8	1.2×10^4	6.2×10^6	1.9×10^{-10}	9.5×10^{-7}	0.83			
1.7	9.3×10^3	3.7×10^6	2.1×10^{-10}	1.4×10^{-6}	0.77			
2.5	7.0×10^3	1.1×10^5	1.6×10^{-10}	1.3×10^{-6}	0.80	1.5×10^{10}	1.4×10^{-5}	0.40
3.3	1.8×10^3	3.7×10^3	4.7×10^{-10}	2.8×10^{-6}	0.80	3.6×10^3	5.5×10^{-6}	0.37